Energy

Research article

Validation of thermal imaging as a tool for failure mode detection development

Javier Olarte[1,2,]*, Jean-Luc Dauvergne[2], Alvaro Herrán[2], Nicholas E. Drewett[2], Emilie Bekaert[2], Ekaitz Zulueta[3] and Raquel Ferret[2]

[1] Bcare. C/Albert Einstein 48, 01510 Miñano, Álava, Spain
[2] CIC energiGUNE. C/Albert Einstein 48, 01510 Miñano, Álava, Spain
[3] UPV/EHU. C/Nieves Cano 12, 01006 Vitoria Gasteiz, Álava, Spain

* Correspondence: Email: jolarte@bcaremb.com, jolarte@cicenergigune.com; Tel: +34945297108.

Abstract: The development of tools for examining and predicting battery performance represents a significant challenge for the field of monitoring, as it is dependent on nondestructive evaluation (NDE) techniques to provide key behavior descriptors. As the thermal behavior of a battery impacts its internal chemistry, thermal imaging represents an *in operando* NDE technique capable of providing valuable information to facilitate an understanding of a battery's overall electrochemical performance. However, previous attempts to directly link thermal imaging analyses to internal chemistry have—so far—proved challenging due in part to the complexities of the relationships between the thermal and the electrochemical battery behavior. In this article, we propose and describe a more refined approach in which correlation between thermal imaging results and internal battery reactions is first established, providing a foundation for determining descriptors for developing early fault detection. Here, this approach is experimentally validated, through the use of a combination of electrochemical, *in operando* infrared thermography, and post-mortem analyses, which were undertaken in order to characterize selected lead-acid batteries. These results—and their implications for early fault detection—are discussed, along with the challenges facing *in operando* battery thermal imaging, laying a foundation for developing the understanding vital to future iterative design improvements.

Keywords: lead acid batteries; infrared thermography; failure modes; postmortem; early fault detection

1. Introduction

As the requirements facing batteries increase—both in terms of demand and complexity—the ability to understand, control, and predict battery performance becomes ever more urgent. Given the importance of the thermal effect on batteries' behaviors with respect to a wide range of battery properties, including performance, life span, and—critically—safety, it would seem axiomatic that characterization of battery thermal profiles (particularly with respect to thermal monitoring during cycling) is a crucial part of battery development [1–4]. Indeed, relevant models, which range from simple one-dimensional thermal models to highly complex three-dimensional coupled thermal and electrochemical analyses, show that irrespective of device, non-uniform temperature distributions can be present during operation; often resulting in issues for the devices in question [5–12]. Moreover, due to the critical importance of safety, there has been considerable interest in developing and improving the thermal handling of battery systems—particularly with respect to that undertaken by the battery management system (BMS) [13–16].

This highlights the relevance of temperature with respect to operational and safety analyses for fuel cells and batteries, which is subsequently reflected in the varied and abundant literature produced regarding monitoring the thermal characteristics and behaviors of these devices [17–20]. Consequently, techniques appropriate for the elucidation of a greater understanding of these phenomena are in great demand. It should be no surprise, therefore, that thermal monitoring has become a popular area of research [21]. One increasingly popular analytical tool is infrared thermography (IT), as it is a safe, non-destructive, and contactless technology, which may be used to determine the thermal profile of a battery [20–22]. However, in addition to providing insights into the thermal profile of a battery (i.e. thermal monitoring) it must be noted that IT may also identify hotspots *in situ* (while the battery is still in operation) [21,23]. In many conventional battery systems, hotspots represent an indication of a fault and so, in this way, IT represents a powerful tool—capable not only of thermal monitoring but also the hitherto mostly neglected possibility [21,24] of early fault detection.

In general, nondestructive evaluation (NDE) by infrared thermography may be divided into two methods: 1) passive infrared thermography (PIT) and 2) active infrared thermography (AIT) [25]. In essence, PIT involves detecting abnormal temperature fields—the presence of which may indicate anomalies. This technique, mainly used for qualitative inspection and localization purposes, is relatively simple to implement and has been used to good effect for diagnosis in other fields [26]. By contrast, AIT consists of analyzing the transient heat flux of the thermal scene after its solicitation by an external thermal source, and has proven to be a powerful tool when PIT is too sensitive to variations of surrounding conditions, requires too long a duration, or does not provide sufficient thermal contrast [27]. While AIT does offer advantages over PIT, the simplicity of PIT makes it an ideal starting point for evaluation. Indeed, previous work has demonstrated that PIT in particular may be applied to lead acid batteries in order to successfully detect observable failures [24]. However, it also highlighted the difficulties in attempting to correlate voltage and thermal signal. This may be attributed to the complexities of the internal chemistries and design of the battery system making such attempts at direct correlation extremely challenging.

In order to address this issue, we believe that a refined approach may prove more viable. This may best be summarized as first correlating the battery's thermal behavior—and formation of hotspots in particular—to the internal reactions, before using this understanding to develop the key

descriptors for electrochemical performance prognosis with respect to early fault detection.

In this way, by linking the internal battery reaction to its thermal and electrical behavior, we suggest it will be possible to a) develop a non-destructive early fault monitoring technique; b) develop a refined thermal monitoring tool to ensure smooth and safe battery operation; and c) provide a framework of improved understanding to facilitate future iterative improvements.

However, in order to justify future development of this technique, it is first necessary to demonstrate the added value of such an approach. Thus, in order to validate our proposed technique as a proof-of-concept, we use—for the first time—a combination of in operando thermal imaging, electrochemical measurement, and post-mortem analysis to determine the utility and viability of the proposed technique.

In this work, we describe in detail our experimental methodology which consists of:

1) Gathering a dataset of thermal/electrochemical behaviors of pre-selected lead acid batteries.

2) Using PIT to identify key internal features of interest.

3) Undertaking post-mortem analyses to characterize these identified areas.

4) Correlating the batteries' most relevant internal reactions to thermal behavior, so as to validate the utility of this approach.

5) Examining these proof-of-concept results with respect to applicability of this method to early fault detection in batteries.

Finally, we will summarize the results and discuss in detail the implications with regard to the on-going development of a fault detection model.

2. Methodology

2.1. Criteria for battery selection

Two types of batteries were selected for analysis in this work: systems which are at the beginning-of-life (henceforth 'BoL systems'), having undergone formation cycles only, and systems which have undergone field aging resulting from use in real-world telecommunications powerplant (henceforth 'degraded systems').

These batteries consist of a series of 6 cells, each of which has a grid of alternately 4 anode and 3 cathode plates, each insulated by a glass fiber separator impregnated with electrolyte (see schematic in Figure 1).
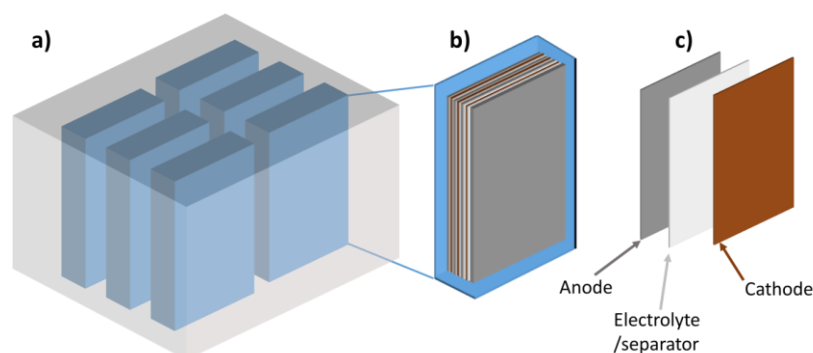
Figure 1. Schematic of a) battery; b) cutaway of cell; c) internal grid structure.

2.2. Experimental setup and protocol

The two selected batteries were placed in a climate chamber, controlled by an Omron E5CC temperature controller, with padded walls to limit environmental reflections (Figure 2). The electrochemical tests were carried out using an Arbin LBT22043 cycler. The cycler's ADC (analog to digital converter) has 24 bit resolution, and was configured to acquire data every minute.

**Figure 2.** Picture of the two batteries in the test chamber.

Both batteries were left at room temperature, in the chamber, until thermal equilibrium with the environment was achieved.

After this period of thermal stabilization, the following protocol was simultaneously applied to both batteries:

- Discharge at 0.1C (−0.45 A) until the voltage reached 10.8 V
- A subsequent 2 h rest step
- Charge at 0.3C (1.35 A) under constant current until the voltage reached 14.7 V
- Charge at 14.7 V (constant voltage) until current is 0,01C (0,045 A)
- Subsequently, a floating mode at 13.6 V for 7.5 hours

During the cycling procedure, the thermal behaviors of the two batteries were simultaneously measured using a FLIR A6752SC infrared camera (3–5 μm, 50 mm, f/2.5 lens). This infrared camera was controlled using the FLIR ResearchIR Max software (Version 4.40.9.30). To ensure thermal data was collected at times in accordance with the electrochemical data, thermal images were acquired every minute.

After selection of the appropriate area for measurement (as denoted in Figure 3b), the total thermal scene was represented by images of size 320×256 pixels (Figure 3a). The experimental thermograms were calculated by averaging, at each time step, of two zones of the thermal scene (131×91 pixels per battery, see Figure 3b).
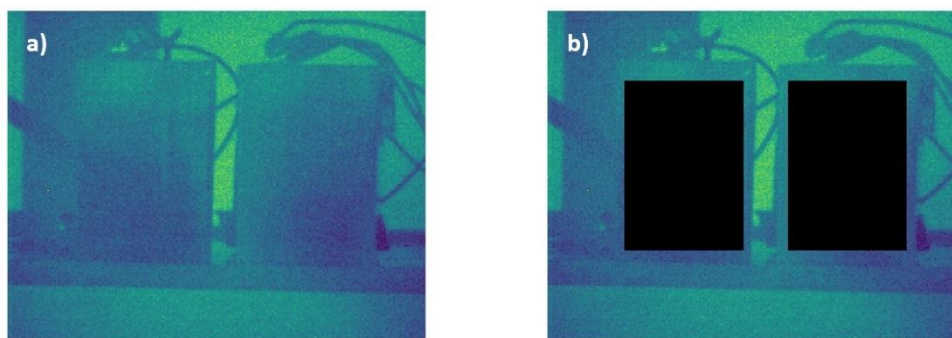
Figure 3. a) Thermal scene of the two studied batteries (t = 0 s); b) two zones, in black, representing the average experimental thermograms calculus. The batteries on the left-side and right-side of each picture corresponds to the BoL and the degraded system respectively.

The recorded data was post-treated using the FLIR ResearchIR Max software and the scientific programming language GNU Octave [28].

Post-mortem analysis was then carried out on relevant samples extracted from the battery. Crystallization was characterized using Scanning Electron Microscope (SEM) FEI Quanta 250. The crystal structures of the lead species present were then identified by X-ray diffraction (XRD) using a Bruker D8 Discover diffractometer (monochromatic Cu Kα radiation, λ = 1.54053 Å), at room temperature, within the 2θ range of 15 −80 °.

3. Results

From the body of experimental data, representative results were selected for characterization. Figure 4 shows the thermal scene at different times during the experiment (total duration c.a. 25 hours).

As expected, the use of passive infrared thermography allowed to detect the damaged battery by means of its excessive energy release (Figure 4, right side). One can notice that the results (images) are given in the arbitrary units of the infrared camera, proportional to the received radiative flux (an excessive energy release appears in yellow in the previous figure). Then, experimental thermograms were calculated for each battery (see 2.2. Experimental setup and protocol). These thermograms were obtained after conversion into apparent temperature using the internal calibration of the infrared camera and by arbitrarily fixing the emissivity of the thermal scene at 0.92. They were also corrected to take into account the variation in temperature of the environment (± 0.7 °C).

The thermograms and the corresponding currents are plotted as a function of time in Figure 5.
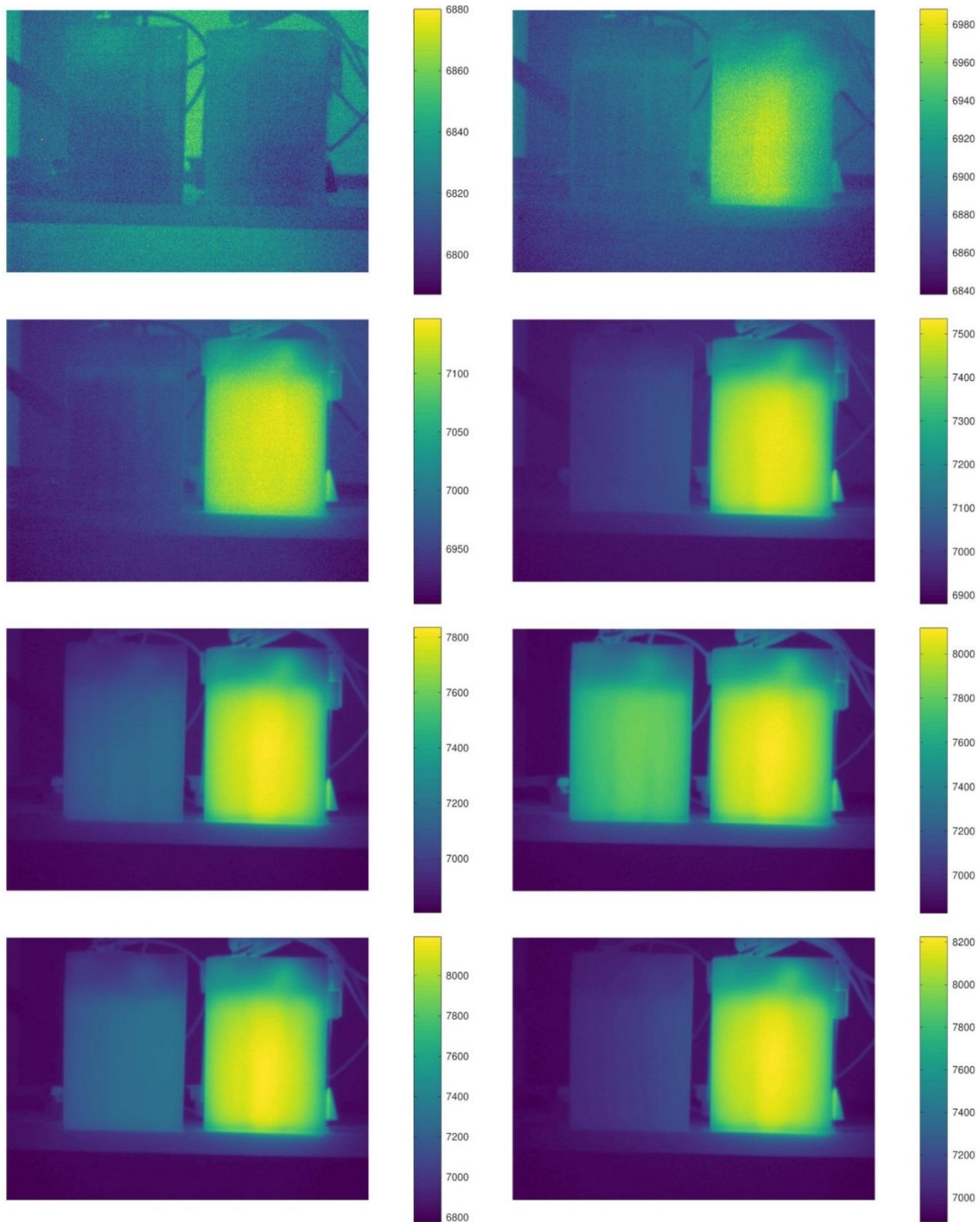
Figure 4. (From left to right and from top to bottom) Thermal scene at time t = 0 s, 10000 s, 20000 s, 30000 s, 40000 s, 50000 s, 60000 s and 70000 s. The batteries on the left-side and right-side of each picture corresponds to the BoL and the degraded system.
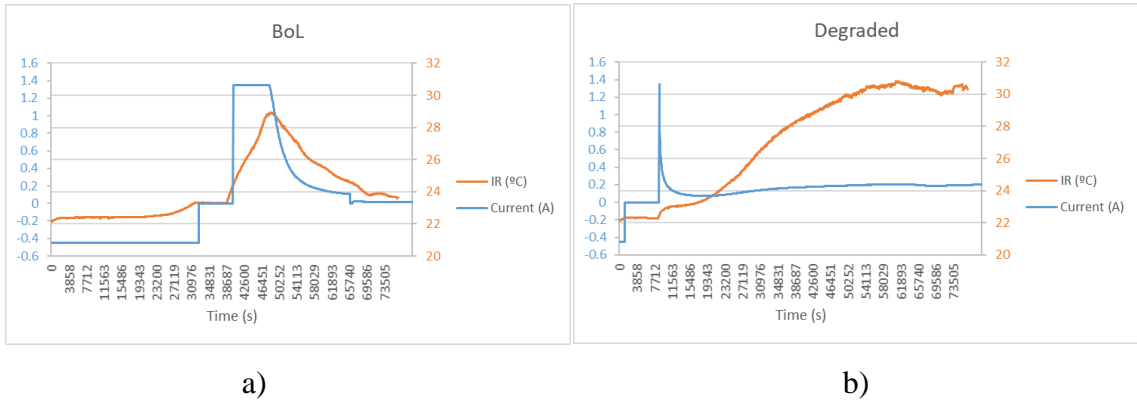
**Figure 5.** Current and infrared profiles for a) BoL and b) degraded systems.

At the end of the experiment (t > 70000 s), an infrared image was taken at each side of the degraded battery. By applying a simple thresholding treatment, the localization of the defective area is easily observed (see Figure 6).
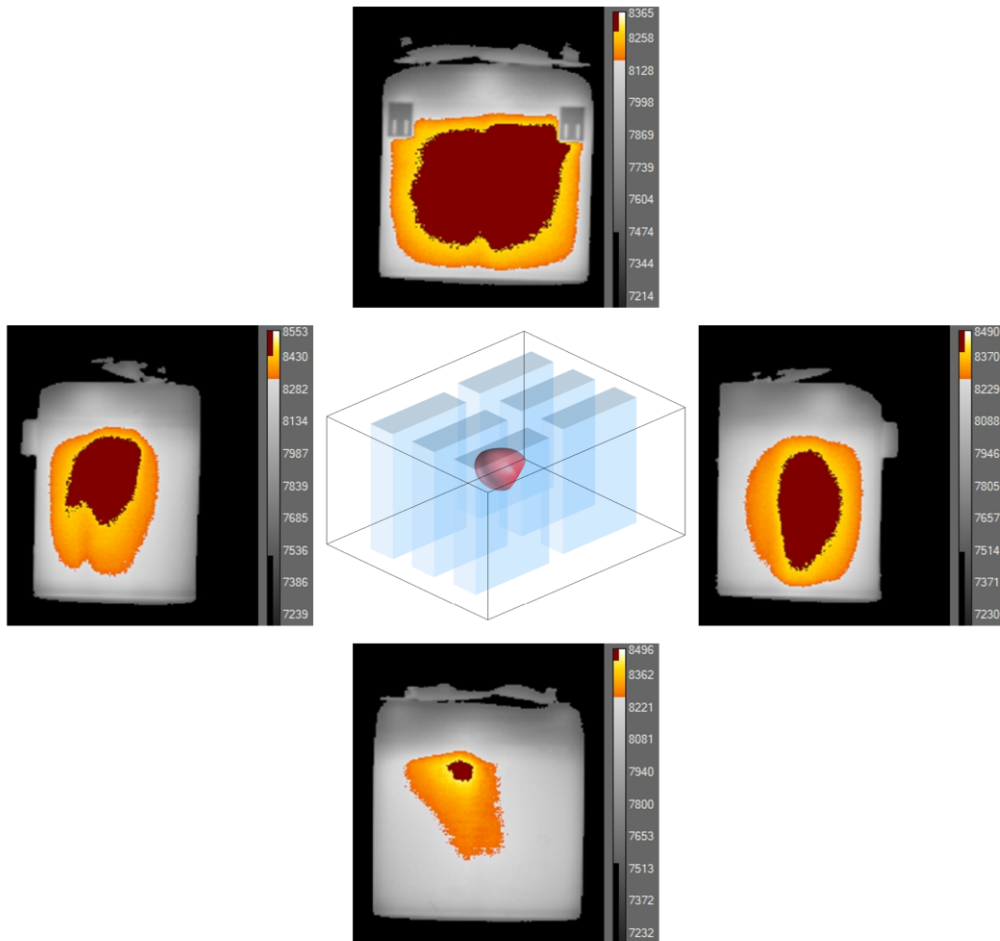
Figure 6. Center, estimated location of defect; surrounding, infrared images of the four faces of the degraded battery.

It should also be noted that the quantitative study of the most emitting zones can provide a powerful tool to refine this location. Indeed, the amplitude of its thermal imprint on a given surface of a battery, as well as its diffusive spread, made it possible to estimate the probable location of a defect. Thus, in the case of the damaged battery studied in this paper, a weaker thermal diffusion observed on the 'left and lower' (Figure 6) faces indicate the proximity of the energy source. In the same way, the higher amplitude of the signal on the 'left' face indicated that the heat source is located near this face. Finally, by exploiting the data of the four faces, the probable location of the defect has been proposed (Figure 6, center). In order to validate the relevance of this approach a post-mortem study was conducted on the defective battery.

In order to ensure relevant post-mortem information was obtained for the aged battery, the points of interest were identified using detailed thermal mapping (see Figure 7). As can be seen, the area is located in upper part of block A, between cell 2 and 3.
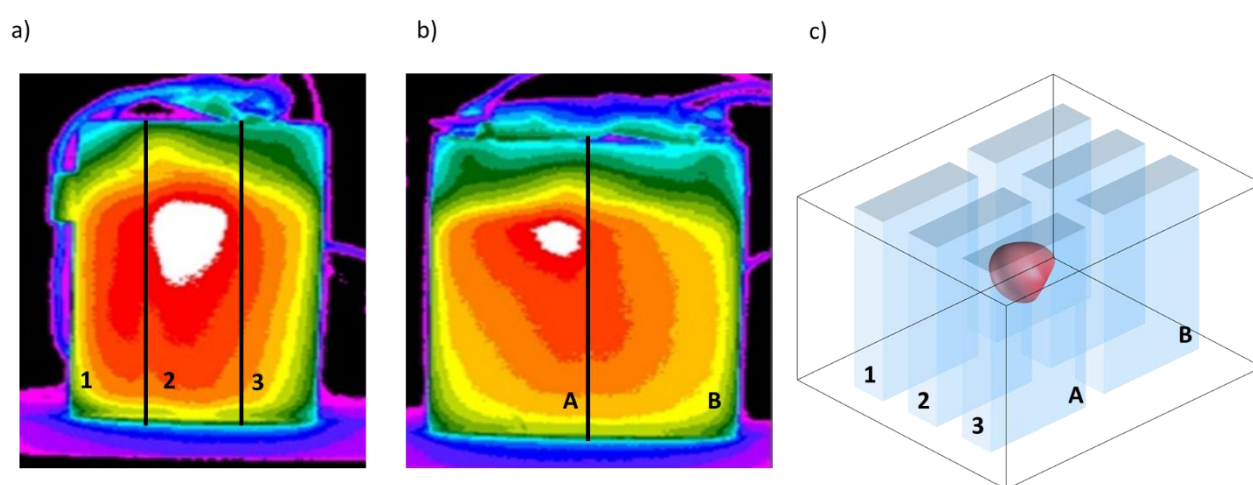

Figure 7. a) Thermal imaging of the battery's edge with cell identification; b) Thermal imaging of the battery's front with block identification; c) schematic of the battery's design with hotpot and the block and cell assignation.

In order to physically access this location, the battery was opened in a well-ventilated fume cupboard using Dremel cutting tools in accordance with safety protocols to ensure good laboratory practice.

Visual inspection (see Figure 8) revealed the anode plate was covered in molten plastic, the area of which corresponded with the estimated defect location. The 3D shape of the effect was, therefore, in good accordance with the highest temperature observed in the hot spot (as identified in the thermal images).
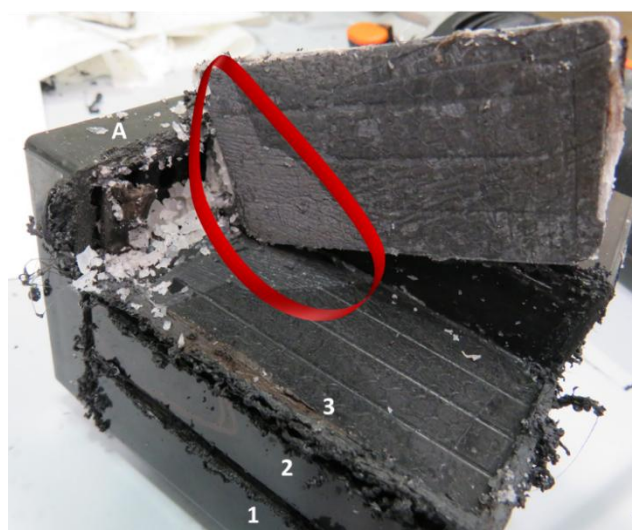
Figure 8. Picture of opened cell with identification of the area of interest.

Upon opening the cell, a more in-depth post-mortem analysis was carried out, including taking XRD and SEM data of areas both in and out of the hotspot (see Figure 9).
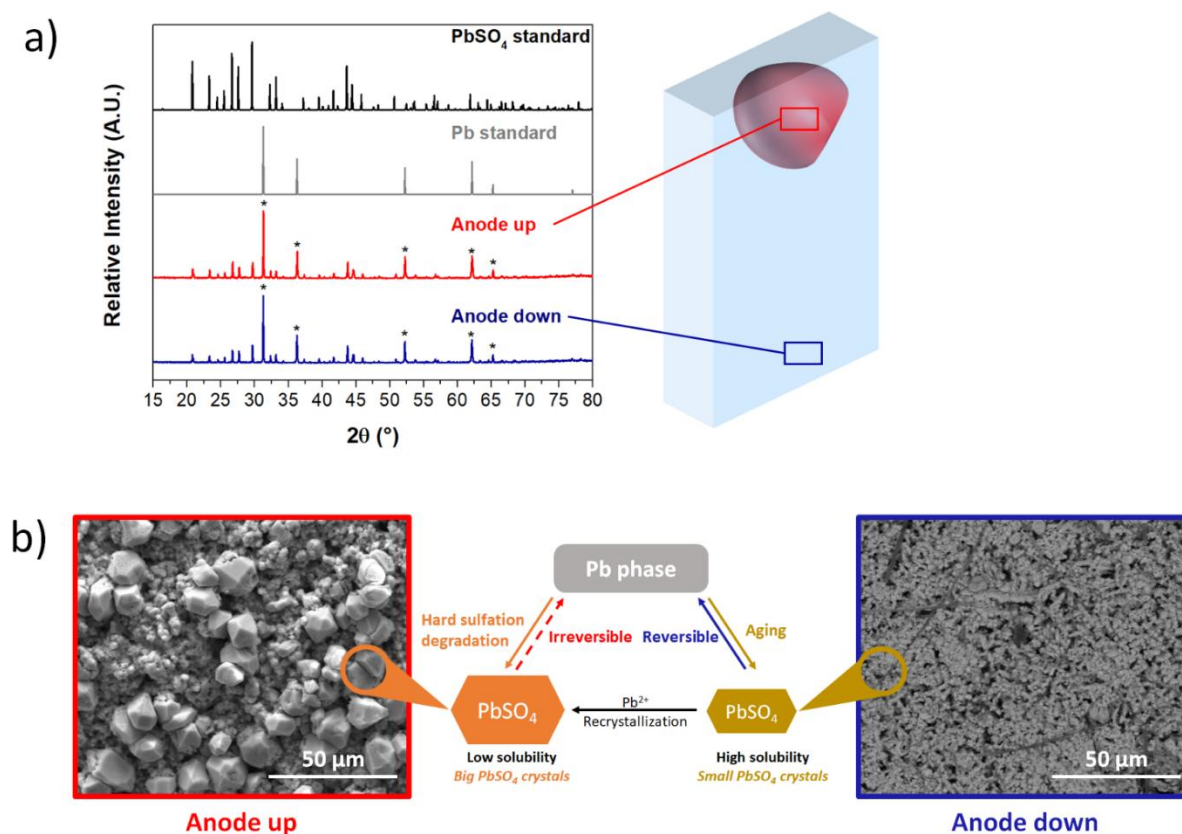
Figure 9. a) XRD results of anode up (red) and anode down (blue), * indicates lead peaks; schematic of location of anode up and down; b) SEM images of anode (red: anode up, hotspot area; blue: anode down, out of hotspot).

Comparison of the XRD (Figure 9a) data to Pb [29] and PbSO$_4$ [30] standards, confirms both are present in both the anode up and down regions. Examination of the SEM data (Figure 9b) reveals some significant difference, however—while the PbSO$_4$ is present at the anode down as small, high solubility crystals, at the anode up region (i.e., at the hotspot) it is present as large, low solubility crystals. The post-mortem analysis of this data, carried out in the discussion section, both explains the results and proposes the mechanism responsible.

4.   Discussion

Examination of the thermal and electrochemical profiles of the batteries (see Figure 5) reveals important information even prior to post-mortem analysis. As can be seen, there is a strong correlation between the current charge/discharge profile and the thermal response for both systems. However, significant differences between the BoL and degraded systems may also be observed. The electrochemical profile of the BoL system followed the typical charge/discharge profile (as described in the manufacturer specifications), and the thermal response showed the expected time shift. By contrast, the degraded system not only exhibited a failed floating mode charge profile, but also an atypically high thermal profile. The combination of this abnormal behavior enabled easy identification of undesirable internal reactions within the battery. In short, comparison of the behaviors of these systems clearly demonstrates the value of this combined electrochemical-thermal analyses as a detection method for identifying areas of interest for in-depth post-mortem characterization.

Given the importance of understanding the effect of the batterýs internal heat generation in order to optimize the systeḿs design, it is important to identify which potential failure mode occurred. The failure modes of lead acid batteries are well reported in the literature [31,32], and include:

• *Hard/irreversible sulfation*—While PbSO$_4$ is a normal product of a discharge at both electrodes, with aging of the battery irreversible sulfation occurs [33]. In essence, the formation of large, insoluble crystals leads to a build-up in their presence and loss of contact between plate and electrolyte, leading to permanent capacity reduction and increased internal resistance.

• *Positive grid corrosion*—positive plate/battery post (usually near the connection to the casing) corrosion restricts current flow, increases internal resistance due to PbO$_x$ passivation layer formation, and so leads to failure from blocked current or cracked casing [34].

• *Electrolyte stratification*—density differences leading to electrolyte separation during rest, resulting in inhomogeneous activity during charge/discharge, increased sulfation in areas with high concentration of acid, and—subsequently - increased wear [35].

• *Water loss/desiccation*—thermally induced evaporation and/or water splitting at high states of charge leading to electrolyte loss, inhomogeneous contact, and thus active and inactive regions leading to localized wear [36].

• *Shedding*—active mass is lost from the plates and collects at the bottom of the battery, which reduces the available active mass (and thus capacity) and—if sufficient mass collects—may cause a short circuit [37].

• *Active mass degradation*—chemical and physical changes in the active mass leading to loss of electrochemically active material and, subsequently, capacity [35].

These mechanisms are well known to result in loss of electrochemical performance within

batteries used in stationary applications.

As seen from our XRD data (Figure 9a), the in-depth post-mortem analyses revealed the presence of $PbSO_4$ crystals at both the anode up and down regions. This observation is, in fact, in accordance with characteristic aging of the battery, as formation of small, soluble, $PbSO_4$ crystals is an inherent part of this process, and typically occurs via an Ostwald ripening mechanism [32].

The SEM data (Figure 9b), however, reveals some significant differences between the natures of the $PbSO_4$ crystals at the anode up and down regions. While the crystals at the anode down region are the small, soluble $PbSO_4$ crystals expected from the typical aging undergone by degraded systems, at the anode up region (the location of the hotspot) we see the large, insoluble, $PbSO_4$ crystals associated with *hard sulfation* degradation [31].

This is a key point, particularly when combined with the visual inspection—which demonstrated dry regions in the anode up area, indicating water loss and desiccation. While determining the exact initial cause of the degradation would require further in-depth analyses beyond the scope of this work (and so are reserved for a future publication focusing on this topic), the information obtained from this combined post-mortem/thermal analysis alone is more than sufficient for us to propose that the following general processes are responsible:

a)   Inhomogeneities in the electrolyte lead to dry regions which hinder $PbSO_4$ from dissolving back into the electrolyte, essentially facilitating increased *hard sulfation*.

b)   Recrystallization of $PbSO_4$—from both normal aging and formation in dry regions—leads to the generation of large, insoluble $PbSO_4$ crystals. The build up of these crystals increases localized internal resistance, leading to localized regions of increased temperature.

c)   Localized increases in thermal activity (e.g., the hotspot observed by the thermal imaging) can lead to localized water loss, and increases in inhomogeneities in the electrolyte and *hard sulfation*.

Given that these processes are self-reinforcing, it seems reasonable to assume that the combination led to sufficient *hard sulfation* degradation and loss of contact as to explain the failure of the battery observed in the electrochemistry. Consequently, we can see there is a strong link between the thermal, physical, chemical, and electrochemical responses observed. Indeed, given the strong link between thermal response and generation of insoluble $PbSO_4$ crystals (*hard sulfation*), we can tentatively propose that such thermal analyses may well enable detection of the degradation mechanism prior to system failure—i.e., a pathway to early fault detection.

This, therefore, represents a strong demonstration of our proposed refined methodology incorporating thermal, physical, chemical, and electrochemical analyses. This not only validates our approach, but also provides a strong framework for future characterization and development of analytical methodologies.

5.   Conclusions

In summary, we have proposed using the correlation between internal battery physiochemistry and infrared thermography as a foundation for electrochemistry prognosis. This methodology not only offers facile, early fault detection, but also provides information regarding areas of interest (enabling rational selection of those areas so as to facilitate rapid diagnosis and evaluation). Validation of the link between thermal images and internal battery reactions has been successfully undertaken through a combination of *in operando* PIT and *ex operando* post-mortem characterization. This demonstrates the usefulness of the proposed methodology with respect towards developing

early fault detection and—potentially—the knowledgebase and framework of understanding key to facilitating the rational iterative improvement of batteries.

Nevertheless, some challenges remain before consideration may be given towards utilization in real-world applications. Firstly, in order to gain the most benefit from this work, it will be necessary to extend validation towards other battery systems. Only by generating a sufficiently encompassing dataset will full utilization of this approach become possible. Secondly, the specific set-up used during this validation did require a degree of free space, the repositioning of the battery in order to generate data from all four sides, and required careful selection of infrared camera. However, it is worth noting that the spatial issues will be less problematic in accumulator rooms, where it is possible to achieve sufficient distance between the batteries and the camera. Moreover, the continuing rapid development of infrared imaging technology, combined with advances in determination of feature significance, would seem to suggest that in the near future improved contactless monitoring will be possible with readily available systems. It would seem reasonable to conclude, therefore, that neither of these challenges represents an obstacle to continuing work in this area.

Meanwhile, by demonstrating clearly that there is an advantage to the novel approach of combined post-mortem data and thermal imaging technologies for battery analysis, here carried out for the first time, we take an important first step towards enhancing the characterization of battery systems in general, as well as representing a strong foundation for future analytical and safety investigations. This would not only be a significant advance for the field in and of itself, but also will be key to the development of remote monitoring of batteries and automated validation—particularly with respect to predicative modelling of performance.

Acknowledgments

Conflict of interest

The authors declare no conflicts of interest.

References

1. Doh CH, Kim DH, Kim HS, et al. (2008) Thermal and electrochemical behaviour of C/Li_xCoO_2 cell during safety test. *J Power Sources* 175: 881–885.
2. Zaghib K, Dontigny M, Guerfi A, et al. (2012) An improved high-power battery with increased thermal operating range: $C–LiFePO_4//C–Li_4Ti_5O_{12}$. *J Power Sources* 216: 192–200.
3. Kim HJ, Lee JH, Baek DH, et al. (2017) A study on thermal performance of batteries using thermal imaging and infrared radiation. *J Ind Eng Chem* 45: 360–365.
4. Chatterjee K, Majumdar P, Schroeder D, et al. (2018) Performance analysis of Li-ion battery under various thermal and load conditions. *J Electrochem Energy Convers Storage* 16: 21006–21007.

5. Bharathan D, Pesaran A, Vlahinos A, et al. (2005) Improving battery design with electro-thermal modeling. *In 2005 IEEE Vehicle Power and Propulsion Conference*, 1–8.

6. Kim US, Shin CB, Kim CS (2009) Modeling for the scale-up of a lithium-ion polymer battery. *J Power Sources* 189: 841–846.

7. Wang Z, Li Z, Liu Q (2011) Infrared thermography non-destructive evaluation of lithium-ion battery. *In Proc SPIE*, 81934I1.

8. Kim US, Yi J, Shin CB, et al. (2013) Modeling the thermal behaviors of a lithium-Ion battery during constant-power discharge and charge operations. *J Electrochem Soc* 160: A990–A995.

9. Yi J, Kim US, Shin CB, et al. (2013) Three-dimensional thermal modeling of a lithium-Ion battery considering the combined effects of the electrical and thermal contact resistances between current collecting tab and lead wire. *J Electrochem Soc* 160: A437–A443.

10. Murashko K, Pyrhönen J, Laurila L (2013) Three-dimensional thermal model of a lithium ion battery for hybrid mobile working machines: Determination of the model parameters in a pouch cell. *IEEE Trans Energy Convers* 28: 335–343.

11. Giegerich M, Koffel S, Filimon R, et al. (2013) Electrothermal modeling and characterization of high capacity lithium-ion battery systems for mobile and stationary applications. *In IECON 2013–39th Annual Conference of the IEEE Industrial Electronics Society*, 6721–6727.

12. Yi J, Lee J, Shin CB, et al. (2015) Modeling of the transient behaviors of a lithium-ion battery during dynamic cycling. *J Power Sources* 277: 379–386.

13. Pesaran AA, Keyser M (2001) Thermal characteristics of selected EV and HEV batteries. *In Sixteenth Annual Battery Conference on Applications and Advances. Proceedings of the Conference (Cat. No.01TH8533)*, 219–225.

14. Waldmann T, Bisle G, Hogg BI, et al. (2015) Influence of cell design on temperatures and temperature gradients in lithium-ion cells: An in operando study. *J Electrochem Soc* 162: A921–A927.

15. Zhang X, Klein R, Subbaraman A, et al. (2019) Evaluation of convective heat transfer coefficient and specific heat capacity of a lithium-ion battery using infrared camera and lumped capacitance method. *J Power Sources* 412: 552–558.

16. Keyser M, Pesaran A, Oweis S, et al. (2019) Thermal evaluation and performance of high-power lithium-ion cells. *In NREL/CP-540-26616*, 1–12.

17. Daino MM, Lu Z, LaManna JM, et al. (2011) Through-Plane water transport visualization in a PEMFC by visible and infrared imaging. *Electrochem Solid-State Lett* 14: B51–B54.

18. Obeisun OA, Meyer Q, Robinson J, et al. (2014) Development of open-cathode polymer electrolyte fuel cells using printed circuit board flow-field plates: Flow geometry characterisation. *Int J Hydrogen Energy* 39: 18326–18336.

19. Guo H, Wang MH, Liu JX, et al. (2015) Temperature distribution on anodic surface of membrane electrode assembly in proton exchange membrane fuel cell with interdigitated flow bed. *J Power Sources* 273: 775–783.

20. Robinson JB, Darr JA, Eastwood DS, et al. (2014) Non-uniform temperature distribution in Li-ion batteries during discharge—A combined thermal imaging, X-ray micro-tomography and electrochemical impedance approach. *J Power Sources* 252: 51–57.

21. Robinson JB, Shearing PR, Brett DJ (2016) Thermal imaging of electrochemical power systems: A review. *J Imaging* 2: 1–20.

22. Keil P, Rumpf K, Jossen A (2013) Thermal impedance spectroscopy for Li-ion batteries with an IR temperature sensor system. *In 2013 World Electric Vehicle Symposium and Exhibition (EVS27)*, 1–11.

23. Zhang G, Tian H, Ge S, et al. (2018) Visualization of self-heating of an all climate battery by infrared thermography. *J Power Sources* 376: 111–116.

24. Vantuch T, Fulneček J, Holuša M, et al. (2018) An examination of thermal features' relevance in the task of battery-fault detection. *Appl Sci* 8: 1–16.

25. Maldague XPV (1993) *Nondestructive Evaluation of Materials by Infrared Thermography*. Springer Science & Business Media.

26. Grinzato E, Vavilov V, Kauppinen T (1998) Quantitative infrared thermography in buildings. *Energy Build* 29: 1–9.

27. Hung YY, Chen YS, Ng SP, et al. (2009) Review and comparison of shearography and active thermography for nondestructive evaluation. *Mater Sci Eng R Reports* 64: 73–112.

28. Eaton JW, Bateman D, Hauberg S, et al. (2019) GNU Octave version 5.1.0. Available from: https://www.gnu.org/software/octave/doc/v5.1.0/.

29. Bouad N, Chapon L, Marin-Ayral R-M, et al. (2003) Neutron powder diffraction study of strain and crystallite size in mechanically alloyed PbTe. *J Solid State Chem* 173: 189–195.

30. Filatov S, Bendeliani N, Albert B, et al. (2005) High-pressure synthesis of α-PbO$_2$ and its crystal structure at 293, 203, and 113 K from single crystal diffraction data. *Solid State Sci* 7: 1363–1368.

31. Pavlov D, Nikolov P (2012) Lead–carbon electrode with inhibitor of sulfation for lead-acid batteries operating in the HRPSoC duty. *J Electrochem Soc* 159: A1215–A1225.

32. Yang J, Hu C, Wang H, et al. (2017) Review on the research of failure modes and mechanism for lead–acid batteries. *Int J Energy Res* 41: 336–352.

33. Wagner R (1995) Failure modes of valve-regulated lead/acid batteries in different applications. *J Power Sources* 53: 153–162.

34. Glaize C, Genies S (2012) *Lead and Nickel Electrochemical Batteries*. Wiley.

35. May GJ, Davidson A, Monahov B (2018) Lead batteries for utility energy storage: A review. *J Energy Storage* 15: 145–157.

36. Culpin B, Rand DAJ (1991) Failure modes of lead/acid batteries. *J Power Sources* 36: 415–438.

37. Brik K, ben Ammar F (2013) Causal tree analysis of depth degradation of the lead acid battery. *J Power Sources* 228: 39–46.